ELSEVIER

Available online at www.sciencedirect.com

SCIENCE DIRECT®

Microelectronics Reliability 46 (2006) 270–286

MICROELECTRONICS RELIABILITY

www.elsevier.com/locate/microrel

Introductory Invited Paper

# The negative bias temperature instability in MOS devices: A review

J.H. Stathis *, S. Zafar

*IBM Semiconductor Research and Development Center (SRDC), Research Division, TJ Watson Research Center, P.O. Box 218, Yorktown Heights, NY 10598, USA*

Received 27 July 2005
Available online 23 September 2005

**Abstract**

Negative bias temperature instability (NBTI), in which interface traps and positive oxide charge are generated in metal–oxide–silicon (MOS) structures under negative gate bias, in particular at elevated temperature, has come to the forefront of critical reliability phenomena in advanced CMOS technology. The purpose of this review is to bring together much of the latest experimental information and recent developments in theoretical understanding of NBTI. The review includes comprehensive summaries of the basic phenomenology, including time- and frequency-dependent effects (relaxation), and process dependences; theory, including drift–diffusion models and microscopic models for interface states and fixed charge, and the role of nitrogen; and the practical implications for circuit performance and new gate-stack materials. Some open questions are highlighted.
© 2005 Elsevier Ltd. All rights reserved.

## 1. Introduction

The purpose of this review is to bring together much of the latest information and recent developments in understanding of NBTI. There has recently been an explosion of publications on this subject (see, for example, [1,2]). We aim to be as up-to-date as possible and to have this review represent the state of the field, but the rapid pace of development in this topic means that by the time this review appears in print it may easily miss some important new development. Recent experimental work, especially in the area of AC stress and the associated recovery phenomena, will almost certainly lead to improved understanding in the near future. We have tried to present an objective and unbiased review of the work of many groups, in spite of the fact that one of us (SZ) is the author of a particular NBTI model. It is hoped that this review may help to stimulate additional work by highlighting some areas of disagreement and unresolved issues.

This review is organized as follows: Section 2 describes the experimental observations which characterize NBTI. This section includes sub-sections on basic and novel observations and methods, and on process dependencies. Section 3 deals with models, comparing and contrasting the various theories describing NBTI. This section covers macroscopic drift/diffusion models and microscopic models, including the role of nitrogen. Section 4 treats the practical implications of NBTI, including the performance degradation of circuits and the implications for new gate-stack materials. Finally, Section 5 summarizes some of the many open questions.

* Corresponding author. Tel.: +1 914 945 2559; fax: +1 914 945 2141.
*E-mail address:* stathis@us.ibm.com (J.H. Stathis).

0026-2714/$ - see front matter © 2005 Elsevier Ltd. All rights reserved.
doi:10.1016/j.microrel.2005.08.001

## 2. The phenomenon of NBTI

### 2.1. Basic observations and methods

We begin with a description of the more rudimentary aspects of the NBTI phenomenon. These have already been extensively reviewed by others [3,4], so we give here only a brief overview.

The name, negative bias temperature instability (NBTI), refers to the generation of positive oxide charge and interface traps in metal–oxide–silicon (MOS) structures under negative gate bias, in particular at elevated temperature. First reported by Miura and Matukura [5], and further characterized by researchers at Bell Laboratories [6,7], Fairchild Semiconductor [8], and RCA Laboratories [9], the effect was remarkable because an increase in positive charge under negative gate bias implicated a mechanism distinct from the migration of mobile ions which were of much concern in these early MOS studies. (Fig. 1). In terms of practical impact on field-effect transistors (FETs), the greatest impact of NBTI occurs on p-FET devices since only those experience a uniform negative bias condition during typical CMOS circuit operation (Fig. 2).

The early studies outlined the following basic features of NBTI-induced degradation: A broad interface state density peak near mid-gap or in the lower half of the gap [7,10], approximately equal amounts of positive oxide charge and charge in interface states [8], de-trapping or relaxation after removal of bias, [10,11] power-law dependence on time with exponent ~0.2–0.3 [12,13] and on voltage or oxide field with exponent ~2–3 [13], and thermally activated behavior [13] with activation energies from 0.06 to 0.2 eV reported [10,14–16]. Similar amounts of positive charge and interface state generation occur for both n- and p-type silicon substrates [8,10], however since the charge in the interface states depends on bias the net effect on threshold voltage, $\Delta V_t$, is greater for p-FETs, because in this case the positive oxide charge and positive interface charge are additive [13]. This is another reason why NBTI is of greater practical concern for p-FET devices compared to n-FET. In any case, the net contribution to threshold voltage shift will be

$$\Delta V_t = q(\Delta N_{\mathrm{it}} + \Delta N_{\mathrm{f}})/C_{\mathrm{ox}} \quad (1)$$

where $q$ is the electron charge, $C_{\mathrm{ox}}$ is the oxide capacitance, $N_{\mathrm{it}}$ is the density of charged interface states and $N_{\mathrm{f}}$ is the density of fixed charge or slow oxide traps, i.e., those whose occupancy cannot follow rapid changes in the Fermi level $E_{\mathrm{f}}$.

The characterization of NBTI typically entails standard MOS techniques, such as capacitance–voltage, charge pumping, FET parameter extraction, etc. A

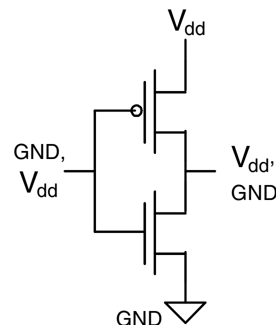


Fig. 2. Bias conditions during circuit operation of a CMOS inverter. With input at ground, output is high and the p-MOS device (top) is under uniform negative gate bias with respect to its substrate. With input high, output is at ground and the n-MOS device (bottom) is under uniform positive bias.

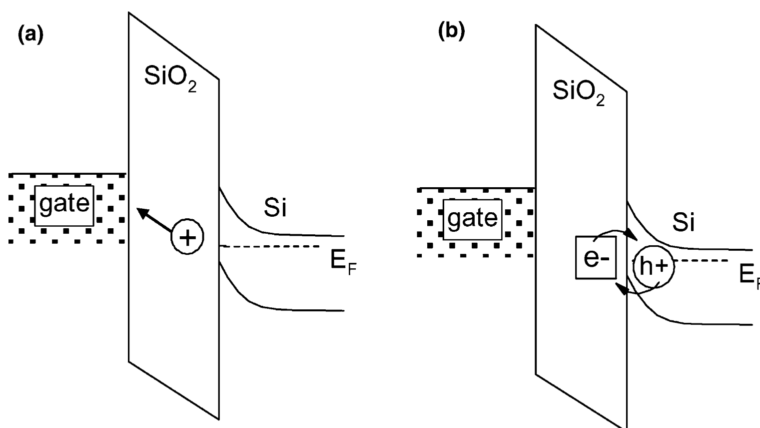


Fig. 1. Effect of negative gate bias on MOS capacitor. (a) Positive ion drift causes a reduction in the net amount of positive charge near the $Si/SiO_2$ interface. The resulting flat band shift is *positive*. (b) Charge exchange with the Si substrate, either hole trapping or electron de-trapping, causes an increase in the net positive charge at the $Si/SiO_2$ interface. The resulting flat band shift is *negative*.

negative bias is applied to the gate of the sample under test (either a capacitor or transistor structure), with interruptions at desired intervals for device characterization. During the stress all other terminals (substrate, source, and drain) are held at ground potential. In this way, the bias condition represents the situation experienced by the p-FET in a CMOS inverter or logic gate with input low (see Fig. 2). Typical results for $\Delta V_t$ as a function of stress time are shown in Fig. 3. Long-channel and wide devices (~0.5 μm or larger in each dimension) may be used in order to increase the statistical certainty [17] and to focus on the characterization of the oxide itself without potential complications from process effects near the device edges. However, a detailed study of channel length and width dependence can be important for actual technology qualification [18].

The criterion for device failure is circuit-dependent, but is often benchmarked at 50 mV shift [4] or $\Delta I_{ds}/I_{ds} \sim 10\%$. The generation of $10^{11}\,\mathrm{cm}^{-2}$ positively charged defects results in a threshold voltage shift of $\Delta V_t = 5\,\mathrm{mV} \times t_{ox}$ (nm) where $t_{ox}$ is the oxide thickness. With technology scaling, the thickness of the gate dielectric has continually decreased, and therefore $\Delta V_t$ is proportionally reduced. However, several effects conspire to bring NBTI to the attention of device and circuit designers: first, the operating voltage has not scaled as rapidly as gate oxide thickness, resulting in higher fields which enhance the NBTI [4]; second, device threshold voltage scaling has not kept pace with operating voltage, which results in larger percentage degradation of drive current for the same $\Delta V_t$ [19]; and third, the addition of nitrogen into the gate dielectric for gate leakage reduction and control of boron penetration has had the side effect of increasing NBTI [20].

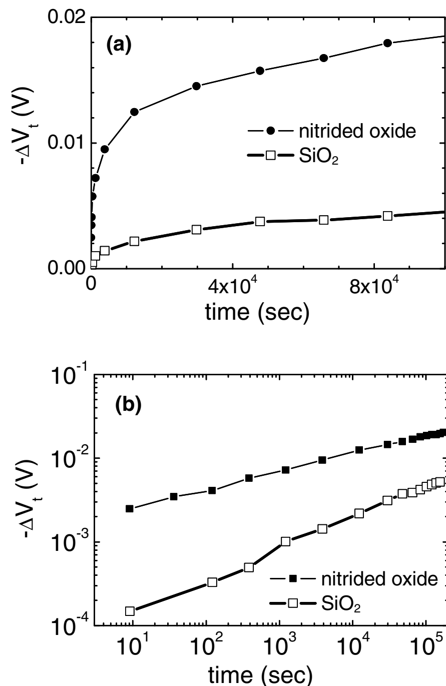


Fig. 3. Typical result for threshold voltage shift resulting from p-MOS negative bias stress, (a) linear plot; (b) same data on log–log plot showing power-law behavior.

### 2.2. Novel and advanced observations and methods

The recovery, or relaxation, of NBTI [11] has received increased attention recently as NBTI has come to the forefront of critical reliability phenomena in advanced CMOS technology. Under actual AC operation conditions this recovery phenomenon, sometimes referred to as Dynamic NBTI, may result in a less severe net shift in device parameters over the long term, compared to the expected DC result [16,21,22]. This is illustrated in Fig. 4 showing the threshold voltage shift as a function of time, with intervals of stress (gate negative, i.e., p-FET in inversion) and recovery (gate positive, i.e., p-FET off). Large recovery of $V_t$ occurs during the off stage. At each stress interval the $V_t$ degradation at first returns quickly, then continues to degrade more slowly. Over the long term, the net degradation is less than for same DC equivalent stress time without the relaxation intervals. The ratio of AC to DC degradation is affected by the duty cycle. At 50% duty cycle, the net $\Delta V_t$ is less than one-half of its DC value, with little or no frequency dependence up to 500 kHz according to some reports [23–26] but then decreasing further above 2 MHz [27]. Since NBTI follows a shallow power-law dependence on time, i.e., $t^n$ ($n = 0.2$–$0.3$), a 2× decrease in degradation results in better than 10× longer lifetime. At lower duty cycle, the improvement can be as much as 100× [25].

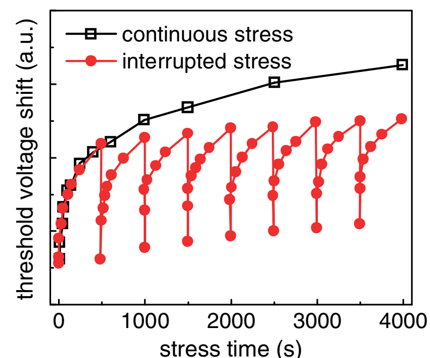


Fig. 4. Threshold voltage shifts in a 2 nm nitrided oxide for a continuous stress (open squares) at $V_g = -2.5$ V and for interrupted stress with an positive bias interval ($V_g = +1.5$ V) (filled circles). After [16].

Even for a DC stress, accurate quantitative assessment needs to correctly take relaxation into account, lest it distort the measurement results, for correct extrapolation of NBTI lifetime. The usual interrupted stress techniques can result in uncharacterized delays between stress and measurement, leading to errors and uncertainty in the degradation rate. It has been shown that the apparent power-law exponent for the time dependence increases if the delay increases between the removal of stress voltage and the measurement of device parametric degradation, as shown in Fig. 5 [21,28,29].

These results indicate that even a nominally 'DC' experiment such as Fig. 3, or the upper curve in Fig. 4, may be distorted by relaxation effects since each measurement point involves removing the stress, however briefly [30]. One suspects that many results in the literature may be influenced by hitherto uncharacterized relaxation effects. To avoid this, the measurement interval should be kept as short as possible, but since $\Delta V_t$ recovers very quickly at short relaxation times this may be difficult in practice. Measurement times below 1 s may be fairly easily achieved [29,31] by doing a single-point measurement of the drain current near threshold in the linear region ($I_d^{lin}$), rather than a full $I_d$–$V_g$ sweep, and using the known initial $I_d$–$V_g$ characteristics to estimate $\Delta V_t$ from $\Delta I_d^{lin}$ at fixed $V_g$. The threshold voltage recovery time dependence is shown in Fig. 6. The recovery follows a log($t$) dependence down to at least 1 ms [31], so extrapolating to zero delay is not possible.

To avoid recovery effects altogether, it is possible to measure degradation in real-time by monitoring the drain current ($I_{ds}$) with a small (~50 mV) drain voltage during stress [29,31]. By applying a small gate voltage modulation $\delta V_g$ (~100 mV) it is likewise possible to measure the transconductance $g_m(t) = dI_{ds}/dV_g$ continuously at stress condition [32,33]. This relation can be numerically integrated to deduce $\Delta V_t = \int dI_{ds}/g_m$. Another possible technique is to monitor the frequency degradation of a ring oscillator during stress [34]. The transistors in the ring should be designed with long channel length to avoid additional degradation from hot carrier effects. Circuit simulation is then required to relate the observed frequency shift to a threshold voltage shift.

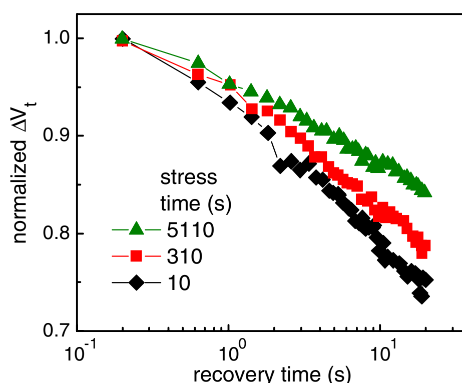


Fig. 6. Recovery of threshold voltage shift ($\Delta V(t)/\Delta V_t(0.2$ s)) as a function of recovery time after stress. After [29].

As stated in Eq. (1), two components separately contribute to $\Delta V_t$, the interface states ($N_{it}$) and oxide 'fixed' charge ($N_f$). It is possible to distinguish these components, e.g., by using charge pumping (CP) to measure the $N_{it}$ contribution separately. The time dependences of $\Delta N_{it}$ and $\Delta V_t$ may differ [14,35], with the power-law exponent for $\Delta N_{it}$ remaining close to 1/4 while $\Delta V_t$ or $\Delta N_f$ have a more shallow time dependence, and the activation energies for $\Delta N_{it}$ is higher than for $\Delta V_t$ or $\Delta V_f$ (0.2–0.16 eV vs. 0.15–0.06 eV) [14,16,30]. The activation

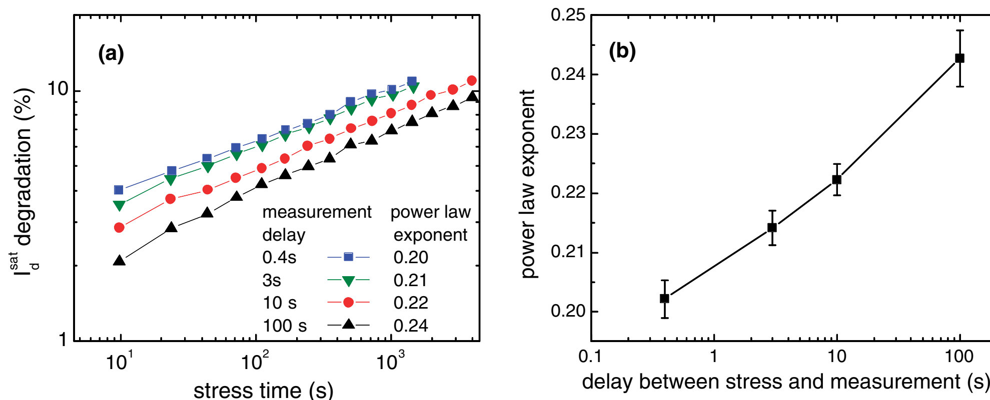


Fig. 5. (a) NBTI degradation vs. stress time for various delays between stress interruption and measurement, (b) power-law slope vs. delay time. After [28].

energy for interface state creation is consistent with older data on trap creation in $SiO_2$ [36], and the lower temperature dependence for the net threshold voltage shift is consistent with hole trapping [16]. In the future, it may become more important to try to distinguish defect generation from hole trapping at existing defects.

Some researchers also found that as a function of frequency, $\Delta N_{it}$ remains constant but $\Delta V_t$ decreases (Fig. 7) [37]. This implies that the $N_f$ component (presumably, hole trapping) becomes less important at higher frequency. Consistent with this, they also reported that the recovery of $\Delta N_{it}$ under positive bias is much less than that of $\Delta V_t$, as shown in Fig. 8 [15,16,30,35,37–40]. From this it may be concluded that re-passivation of interface states is a negligible part of the relaxation mechanism, and that hole de-trapping dominates this process.

Taken together, the above results tend to a consistent picture: the shallower time dependence of $\Delta N_f$ explains the shallower time dependence for shorter delay times where $N_f$ has not yet relaxed. Other researchers, however, have observed a different behavior, e.g., $N_{it}$ recovery comparable to that of $V_t$ [25,41–43] or $I_d^{lin}$ [31]. Some studies found recovery to be independent of the magnitude or sign of the applied bias during recovery, suggesting a neutral species is involved, e.g., re-passivation of $N_{it}$ by atomic hydrogen [31], while others report that the passivation is enhanced with positive bias, suggesting either a positive species such as $H^+$ being pushed back toward the $Si/SiO_2$ interface, or electrons from the substrate neutralizing the trapped holes [25,42,43].

Temperature-dependent stress and recovery experiments indicate that the recovery is slower at higher temperature [31,43]. At room temperature and below, nearly 100% recovery of $I_d^{lin}$ degradation can be obtained [31], which suggests that hole trapping dominates in this regime, whereas permanent interface trap creation requires higher temperature. For a thinner oxide, where sufficient tunneling current may flow to cause the generation of additional traps and interface states, the room temperature recovery is less than 100% [44].

The power-law time dependence used in most NBTI descriptions may not be strictly valid, especially for long-time stress where saturation is sometimes observed [45–48]. An example of this is shown in Fig. 9. In these data the power-law exponent changes from ~0.25 initially (stress time ~100 s) to 0.16 at $10^6$ s stress time, and the saturation level is voltage dependent.

Saturation such as shown in Fig. 9 may have important implications for lifetime assessment [45,48,49]. The end-of-life degradation will be determined by the saturation level, if the saturation time is shorter than the product life time (e.g., 10 years), rather than the extrapolation from short time stress data. This is illustrated schematically in Fig. 10, which shows lifetime increasing more rapidly at low voltage because of the saturation and decreasing power-law slope.

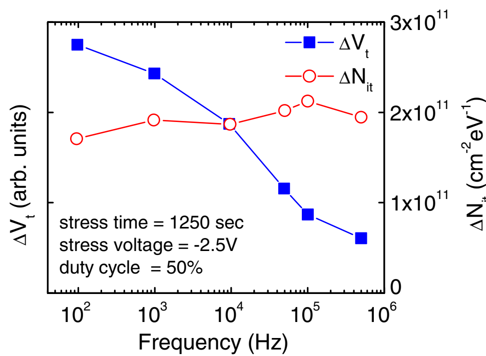


Fig. 7. $V_t$ shift (filled squares) and interface trap density change (empty circles) for $V_g = -2.5$ V stress for 1250 s at different frequencies (duty cycle 50%). After [37].

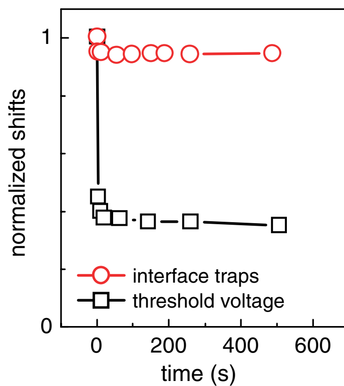


Fig. 8. Relative shifts for the interface trap density and the threshold voltage vs. relaxation time following 2500 s NBTI stress. After [37].

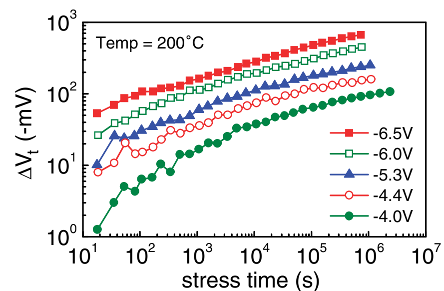


Fig. 9. $\Delta V_t$ vs. stress time for various stress voltages on a 6.7 nm oxide. Degradation saturates as stress time increases. Similar saturation also reported for thin (1.75 nm) oxide. After [45].

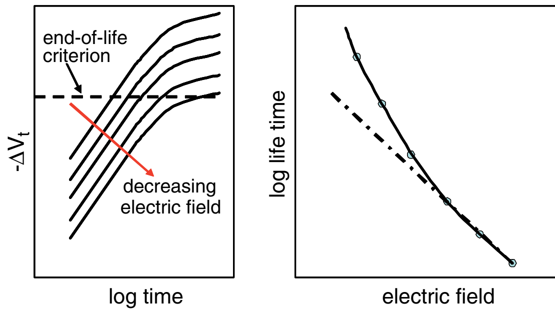


Fig. 10. Schematic illustration to explain the dependence of lifetime on $E_{ox}$. After [45].

### 2.3. Process dependencies

The effect of process conditions on NBTI has been the subject of extensive but largely empirical study. Of most interest lately is the effect of nitrogen, which will be the subject of a separate section.

It was established early on that hydrogen and/or water play a large role in NBTI [9,50] and that water released from intermetal dielectrics in the upper layers of an integrated circuit can increase NBTI. A silicon nitride barrier ($Si_3N_4$) layer above the transistors and other barrier materials can be used to control this effect [51,52]. Excess hydrogen annealing will also increase NBTI [53,54]. Another impurity which has been shown to increase NBTI is chlorine [55], while fluorine has a beneficial effect [46,53,56]. Replacing hydrogen by its heavier isotope deuterium has been shown to reduce NBTI [20,46,57] consistent with a diffusion process, but this effect has not been consistently reproduced [58]. The possible effect of boron is not clear: one report shows an increase in NBTI due to boron penetration from the gate [18], while another shows the opposite trend [59].

## 3. Theories and models

Theoretical treatments of NBTI may be divided along two lines of investigation: models to explain the dependence on time, temperature, and voltage/field; and microscopic models of the defects responsible for charge, e.g., to identify the charged defects or to understand the origin of nitrogen-enhanced NBTI.

### 3.1. Reaction–diffusion and drift models

From the earliest reports [5] an *electrochemical* reaction (between holes and defects) at the $Si/SiO_2$ interface was put forward as the mechanism for NBTI, although trapping of holes in near-interface states by thermally-assisted tunneling was also considered [9,11]. It is well established that the NBTI phenomenon is not dependent on current flow through the oxide, in contrast to oxide breakdown, although as oxides have become thinner the increasing tunneling current can lead to additional defect generation which may have characteristics similar to NBTI.

Leaving the microscopic details of the electrochemical reaction for later, the time dependence of NBTI has been treated as a reaction–diffusion (R–D) process, schematically expressed as [12,60,61]

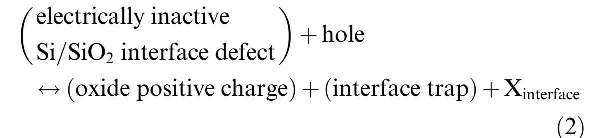

$$\begin{pmatrix}\text{electrically inactive}\\ \text{Si/SiO}_2\text{ interface defect}\end{pmatrix} + \text{hole} \leftrightarrow (\text{oxide positive charge}) + (\text{interface trap}) + \text{X}_{\text{interface}} \quad (2)$$

and

$$\text{X}_{\text{interface}} \overset{\text{diffusion}}{\leftrightarrow} \text{X}_{\text{bulk}} \quad (3)$$

where X represents a mobile species which diffuses away from the interface.

The following two equations then describe the generation of interface traps through reaction and diffusion terms [12,60]:

$$\frac{dN_{it}}{dt} = k_F(N_0 - N_{it}) - k_R N_{it}[\text{X}] \quad (4)$$

$$\frac{dN_{it}}{dt} = -D_X\frac{d[\text{X}]}{dx} + \mu E_{ox}[\text{X}] = -D_X\left(\frac{d[\text{X}]}{dx} - \frac{qE_{ox}}{kT}[\text{X}]\right) \quad (5)$$

where $N_0$ is the initial concentration of interface defects, [X] is the concentration of the mobile species at the interface, and $D_X$ is the diffusion constant, and we have used the Einstein relation $\mu = qD/kT$ where $q$ is the magnitude of the electron charge and $k$ is Boltzmann's constant. The magnitude of the oxide field is $E_{ox}$ and the field is assumed to be in the direction to cause X to drift toward the gate. The right side of Eq. (5) expresses the drift and diffusion of the species X; the second (drift) term is not present if X is uncharged. It is generally assumed that drift/diffusion is the rate-limiting process, so that Reaction (4) may be considered to be in quasi-equilibrium, giving, for $N_{it} \ll N_0$,

$$N_{it}[\text{X}(0,t)] \approx \frac{k_F}{k_R}N_0. \quad (6)$$

The $N_{it}$ growth is then controlled by the diffusion and drift of X, following the usual differential equation

$$\frac{\partial[\text{X}]}{\partial t} = D_X\frac{\partial^2[\text{X}]}{\partial x^2} - \mu E_{ox}\frac{\partial[\text{X}]}{\partial x}. \quad (7)$$

Another useful relation sometimes invoked in treatments of NBTI is the conservation rule [29,61,62]

$$N_{it}(t) = \int [\text{X}]dx \quad (8)$$

in which the integral extends over the oxide thickness. This expresses the fact that each released species X leaves behind one interface state.

These equations become difficult to solve when the boundary conditions for a thin oxide are considered. For an infinitely thick oxide (i.e., oxide thickness $t_{ox} > (4Dt)^{1/2}$ where $t$ is the time), a solution has been given after a lengthy derivation [12] for the case of a *neutral* diffusing species as

$$N_{it} = Rt^{1/4} \tag{9}$$

where $R = 1.16\left(\frac{k_F N_0}{k_R}\right)^{1/2} D^{1/4}$.

A simple but instructive derivation of this time dependence has been given [61]. From classical diffusion the mean distance traveled by [X] is $\bar{x} = (Dt)^{1/2}$. Using Eq. (8) and taking a triangular profile for simplicity gives $N_{it} = 1/2[X(0,t)](Dt)^{1/2}$. Substituting into Eq. (6) we obtain

$$N_{it} = \sqrt{\frac{1}{2}\frac{k_F}{k_R}N_0}(Dt)^{1/4}$$

as well as the relation

$$[X(0,t)] = \sqrt{2\frac{k_F}{k_R}N_0}(Dt)^{-1/4}$$

The derivation of the 1/4 power-law exponent is based on several simplifying analytical assumptions. Numerical simulations have given values that are both somewhat larger [61] and smaller [63].

For finite oxide thickness, if it is assumed that the gate electrode is an absorber for the diffusing species, the rate of $N_{it}$ generation depends inversely on $t_{ox}$ but with the same $t^{1/4}$ time dependence, if X is neutral [60,64]. (A reflecting interface would cause the time dependence to slow down and saturate.) Experimentally, this thickness dependence was verified for $N_{it}$, but $N_f$ was found to be independent of $t_{ox}$ [14,64]. Another description of the effect of oxide thickness has claimed that the time dependence changes to $t^{1/2}$ when the diffusion front of X reaches the gate electrode [61]. Experimentally, a slightly steeper time dependence (not as steep as $t^{1/2}$) has been reported for thin oxides at longer times and attributed to the finite-thickness effect [65]. The break point in this case occurred at fairly low values of degradation ($\Delta V_t < 10$ mV). Most data have not shown this effect.

For charged species, but again assuming infinite thickness, the solution at large $t$ is asymptotically [60]

$$N_{it} = \gamma R t^{1/2} \tag{10}$$

where $\gamma = \frac{\mu E_{ox}}{2\sqrt{D_X}}$. The different time exponent (1/2 vs. 1/4, which is closer to experimental observation) has led most researchers up to now to reject the notion of a charged diffuser [60,61].

The electric field dependence of NBTI arises explicitly in these treatments only for charged diffusing species, Eq. (5). If X is neutral, then the field dependence must be contained in the details of the electrochemical reaction, Eq. (2). If the positive charge in the oxide is located a distance $d$ from the Si/SiO$_2$ interface, the enthalpy of reaction will be $\Delta H = q(\Delta H_0 - dE_{ox})$, giving an exponential field dependence $\propto \exp(qdE_{ox}/kT)$ [12]. A related idea is that in the presence of an electric field the dissociation activation energy of the Si–H dipole is reduced, again giving an exponential voltage dependence [66]. This form is used by some groups [63], while an empirical power-law form form such as $E_{ox}^{3/2}$ [14,64] or $E_{ox}^4$ [41] (Fig. 11) is often used by others.

A correct treatment of the drift/diffusion of X should include the dispersive nature of this process in an amorphous material [29,48,49,62,67]. Dispersive transport arises when the mobile species experiences a broad distribution of barrier heights, leading in turn to an exponentially broad distribution of hopping times.

For dispersive transport, the diffusion 'constant' may be replaced by the time-dependent expression $D_X(\nu t)^{\beta-1}$, where $\beta = kT/E_0$ is the dispersion parameter ($0 \leqslant \beta \leqslant 1$), $E_0$ is a characteristic energy scale, and $\nu$ is a characteristic frequency, and Eq. (7) can be replaced by [29,62]

$$[X] = \frac{1}{\nu}D_X(\nu t)^{\beta}\left[\frac{\partial^2[X]}{\partial x^2} - (qE_{ox}/kT)\frac{\partial[X]}{\partial x}\right] \tag{11}$$

which can be solved straightforwardly [29,62] and together with Eqs. (5) and (6) leads to expressions for the time dependence of $N_{it}$,

(a) for a neutral species,

$$N_{it} = R(\nu t)^{\beta/4} \tag{12}$$

where $R = \left(\frac{k_F}{k_R}\right)^{1/2}\left(\frac{D}{\nu}\right)^{1/4}$ and

(b) for a charged species, in the limit of high field or long time where the drift term dominates,

$$N_{it} = R(\nu t)^{\beta/2} \tag{13}$$

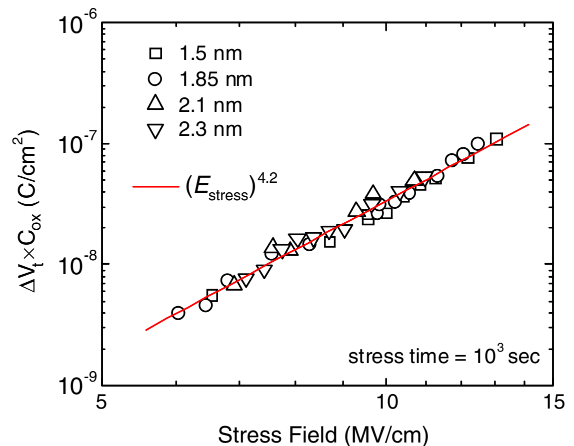


Fig. 11. Field dependence of NBTI. After [41].

where $R = \left(\frac{k_F}{k_R}\right)^{1/2}\left(\frac{\mu E_{ox}}{v}\right)^{1/2}$. In the classical limit $\beta = 1$ and the time dependences in Eq. (12) and Eq. (13) revert to 1/4 and 1/2, respectively, as found earlier for neutral vs. charged species. However, for dispersive transport the value of $\beta$ may be typically ~0.3–0.5, so that it is not necessary to rule out the possibility of charged species as previously believed based on classical (Gaussian) diffusion results.

An alternative approach [48] bypasses solving the diffusion problem, and uses statistical mechanics to write Eq. (6) as

$$[X_{interface}] = N_i e^{-E_i/kT}((N_0/N_{it}) - 1) \tag{14}$$

where $E_i$ is the energy required to generate interstitial species X at the interface and $N_i$ is the density of available interstitial sites. Adopting the view that X is positively charged so that the drift term dominates and assuming the dispersive transport expression for the mobility, Eq. (5) becomes

$$\frac{dN_{it}}{dt} = D_X(vt)^{\beta-1}\frac{qE_{ox}}{kT}N_i e^{-E_i/kT}((N_0/N_{it}) - 1) \tag{15}$$

which can be integrated to yield

$$\Delta N_{it} - N_0 \ln\frac{N_0}{N_0 - \Delta N_{it}} = -R(vt)^{\beta} \tag{16}$$

where $R = \frac{1}{\beta v} D_X \frac{qE_{ox}}{kT} N_i e^{-E_i/kT}$.

This gives $\Delta N_{it} = R(vt)^{\beta}$ at early times, and at long times becomes a stretched exponential,

$$\Delta N_{it} = N_0(1 - \exp(-R(vt)^{\beta}/N_0)). \tag{17}$$

In addition this allows some model parameters to be given physical significance, e.g., the saturation time is [48]

$$\tau = v^{-1}(R/N_0)^{-1/\beta} = v^{-1}\left(\frac{N_i e^{E_i/kT} D_X q E_{ox}}{N_0 kT\beta}\right)^{-1/\beta} \tag{18}$$

These various models differ significantly in their predictions, e.g., of the dependence on the mass of the diffusing species through the dependence on the diffusion constant $D \propto 1/\sqrt{m}$. The diffusion models, both Gaussian (Eq. (9)) and dispersive (Eq. (12)), depend on the diffusion constant as $D^{1/4}$, whereas the dispersive drift models depend on either $D^{1/2}$ (Eq. (13)) or linearly in $D$ (Eq. (17)). Experimentally, a reduction of NBTI by a factor of at most 1.5 has been observed in deuterated samples, [20] consistent with Eq. (17). Other experiments [58] showed smaller effects.

The stretched exponential form (Eq. (17)) was previously suggested empirically to fit both NBTI and hot-carrier degradation [68]. This form gives a saturation at long times, as a natural outcome, as might be expected for a process which involves the depassivation of interface defects.

Many NBTI models give expressions only for the interface state density $N_{it}$ (e.g., Eqs. (9), (12), (13), (17), and (19) below), with the implicit assumption that the fixed charge component $N_f$ is uninteresting or trivially related to $N_{it}$ as a proportionality, but experiments (e.g., Figs. 7 and 8) tell us that $N_f$ should be considered more rigorously. One approach [48] is to assume that bulk traps are generated in proportion to $N_{it}$ but that the occupancy of these traps depends on the Fermi level during stress. The result is an expression for the total $V_t$ shift with the same stretched exponential form as Eq. (17), with a saturation value $\Delta V_{max}$ which depends on the stressing field as indicated in Figs. 9 and 10.

The dispersive transport picture predicts a temperature-dependent exponent for the time dependence, via the dispersion parameter $\beta = kT/E_0$. This further leads to a non-Arrhenius temperature dependence, [62] since according to Eq. (12), (13) or (17) at fixed time $\Delta N_{it} \propto v^n$ where $n$ is proportional to $kT/E_0$. Taking the log of this expression yields $\ln(\Delta N_{it}) \propto (kT/E_0)\ln(v)$. Fitting data to this relationship gives a value of $v = 500\ s^{-1}$. This seems rather low, i.e., much less than a typical phonon frequency ($\sim 10^{12}\ s^{-1}$). However, it is consistent with the empirical relation known as the Meyer–Neldel rule commonly observed for dispersive transport in amorphous materials [69,70].

A different approach, again invoking the concept of disorder, starts from the observation that the Si–H bond breaking energy has a broad distribution [37,71]. This results in the following relation:

$$\Delta N_{it} = N_0/(1 + (t/\tau)^{-\beta}) \tag{19}$$

where $\beta = kT/\sigma$ is again a dispersion parameter, $\sigma$ being the width of the energy distribution. The saturation onset time is $\tau = \tau_0\exp(E_d/kT)$ where $E_d$ is the Si–H dissociation energy, which may be voltage dependent. At early times Eq. (19) reduces to the power-law form $\Delta N_{it} = N_0(t/\tau)^{\beta}$.

Several models have been published explaining the recovery phenomenon in terms of diffusion of a hydrogenous species back to the $Si/SiO_2$ interface when the generation term is turned off. If the recovery follows the same $t^{\beta}$ time dependence as the generation, then a phenomenological model [72] writes the recovery phase as

$$\Delta V_t^r = \Delta V_{t,i-1}(1 - \alpha(\Delta t)^{\beta}) \tag{20}$$

where $\Delta V_{t,i-1}$ is the shift at the end of the prior stress phase and $\alpha$ is a parameter indicating the fraction which does not recover during a recovery time equal to the previous stress time. The net shift during the next stress phase is then written as

$$\Delta V_{t,i} = R(t_{eff} + \Delta t)^{\beta} \tag{21}$$

where $t_{eff}$ is the time at which a DC stress would have reached the same starting degradation level $\Delta V_t^r$. The net degradation under AC stress can be estimated by

repeating this sequence. Numerical calculations based on the classical diffusion models have been published with similar results [63,73].

An analytic form for recovery, after a stress time $t_{stress}$, has been given for classical (Gaussian) diffusion [73] as

$$N_{it}(t') = N_{it}^0[1 - (t'/2)^{1/2}/(1 + t')^{1/2}] \quad (22)$$

where $t' = t/t_{stress}$ and $N_{it}^0$ is the interface state density at the beginning of relaxation. According to the dispersive diffusion model [29] the asymptotic solution for zero field is

$$N_{it}(t') = N_{it}^0[1 + t'^{(\beta/2)}]^{-1}. \quad (23)$$

This expression behaves approximately logarithmically around $t' = 1$, in agreement with data [29,31,33,43, 44,74].

Unfortunately, none of these models correctly address the fact that many researchers (but not all) agree that the recovery of $V_t$ is dominated by the reduction in the $N_f$ component, with very little or no recovery of $N_{it}$. This argues against any recovery mechanism being described simply as the passivation of Si dangling bonds by hydrogen, and suggests a possible role for hole detrapping by tunneling or thermal emission. This is an area ripe for investigation.

### 3.2. Microscopic models for $N_{it}$ and $N_f$

It is generally believed that the initially electrically inactive surface defect in Eq. (2) comprises a hydrogen passivated Si dangling bond, here denoted Si–H, and that X is hydrogen (atom or proton) or some water-related species, (e.g., OH or $H_3O^+$) [12,50,75]. The interface trap is then supposed to be a silicon dangling bond denoted Si$^\cdot$ which results when H is removed from Si–H. A detailed critical analysis of the proposed reactions has been given [60,64]. Here we simply list the various proposals for the reactants in Eq. (2) (Table 1).

Since in all cases the interface trap is assumed to be Si$^\cdot$, we have not listed this component in the table. Note that the last three models do not posit two separate entities for the interface states and the oxide positive charge; in these models all of the positive charge is in the form of charged interface dangling bonds. According to some viewpoints, therefore, bulk positive charge generation is a separate process involving trapping of holes, not defect generation via a low-field reaction [61,65,79].

The last reaction in Table 1 requires interstitial atomic hydrogen. This reaction is known from radiation damage [80], plasma processing [81], and hot electron injection experiments [36,82]; its possible role in NBTI has only recently been proposed based on first-principles calculations of the properties of H at the $Si/SiO_2$ interface [78].

All the listed reactions, except the last, require a hole. However, attempts to prove this component by varying the hole density at the interface at fixed oxide field (this can be done, for example, by applying a positive substrate bias to the n-type substrate of a p-FET) have seen no variation in the rate of defect generation, unless the substrate bias is greater than ~2 V in which case hot-hole injection may cause additional oxide damage [79,83–85]. This supports the idea that the rate-limiting step is the drift/diffusion of the mobile species away from the interface, rather than the reaction.

It does not appear possible to decide among the possibilities listed in Table 1 purely on the basis of the kinetic behavior alone [60,64]. Therefore we must rely on other criteria, e.g., independent measurements of the species X. However, such criteria have net yielded any definitive answer.

The identification of the interface trap as Si$^\cdot$ (named the "$P_b$ center") is based on an extensive history of electron paramagnetic resonance (EPR; also called electron spin resonance, ESR) studies [75]. The $P_b$ center is an amphoteric defect with electronic levels in the upper and lower portions of the Si band gap, and its reactions with hydrogen, e.g.,

$$\text{Si–H} + \text{H} \leftrightarrow \text{Si}^\cdot + \text{H}_2 \quad (24)$$

have been verified [86–88] Two versions of $P_b$ centers, denoted $P_{b0}$ and $P_{b1}$, are present at the (1 0 0)$Si/SiO_2$ interface, whose physical and electronic structures are still debated [89]. The EPR studies of NBTI are very few [57,76,77].

Table 1
Microscopic reaction models

| Interface defect | Oxide positive charge | X | Refs. | Reaction |
|---|---|---|---|---|
| Si–H + Si–O–Si | $Si^+$ | Si–OH | [12] | Si–H + Si–O–Si + $h^+ \leftrightarrow$ Si$^\cdot$ + $Si^+$ + Si–OH |
| Si–H + $H_2O$ | Same as X | $H_3O^+$ | [76,77,50] | Si–H + $H_2O$ + $h^+ \leftrightarrow$ Si$^\cdot$ + $H_3O^+$ |
| Si–H | Same as X | $H^+$ | [50,63] | Si–H + $h^+ \leftrightarrow$ Si$^\cdot$ + $H^+$ |
| Si–H | $Si^+$ | $H_2$ | [61,63] | Si–H + $h^+ \leftrightarrow$ Si$^{\cdot+}$ + $\frac{1}{2}H_2$ |
| Si–H | $Si^+$ | H | [63] | Si–H + $h^+ \leftrightarrow$ Si$^{\cdot+}$ + H |
| Si–H + $H^+$ (from substrate) | $Si^+$ | $H_2$ | [63,78] | Si–H + $H^+ \leftrightarrow$ Si$^{\cdot+}$ + $H_2$ |

Although these defects may be responsible for a portion of the electrically active interface states, the energy spectrum of $P_b$ centers is different from the dominant hydrogen-induced defects [90], and quantitative studies demonstrate that in some cases less than half of $N_{it}$ can be ascribed to $P_b$ centers. The remaining interface state density is apparently not EPR-active, and its microscopic structure remains unknown.

### 3.3. The role of nitrogen

Beginning in the 1980s, many groups began adding nitrogen to gate oxides as a way of reducing boron diffusion from the pMOS gate into the channel, and to improve low-field breakdown problems. For ultra-thin oxides (~3 nm or less) nitrogen also is commonly used to increase the dielectric constant and reduce the direct-tunneling leakage current. Silicon oxynitride can improve reliability by acting as a blocking barrier to impurities such as B, $Na^+$, $H_2O$, OH, H, and $H^+$, similar to silicon nitride. However, it also has increased trapping compared to $SiO_2$ [91]. Earlier studies on relatively thick nitrided oxides (~350 Å) found promising results for negative bias stress [92] but for thinner oxides (<100 Å) used in current technology the addition of N to the gate oxide has a serious adverse effect on NBTI [20,46,58,83], as illustrated in Fig. 3.

The nitrogen-enhanced NBTI has a lower activation energy (~0.1 eV) compared to $SiO_2$ (~0.2 eV) [20,83,93] and also a shallower time dependence [83]. One possible explanation for the enhancement is that nitrided oxides contain more water [41].

Comparing pure $SiO_2$ vs. oxynitride films (SiON), the recovery of $V_t$ during positive bias stress is also greater for oxynitride [15,25,40]. If recovery is associated primarily with detrapping of holes, this suggests that enhanced hole trapping is a significant contributor to the nitrogen-enhanced NBTI [15,30,40].

Impurity effects reported for $SiO_2$ (i.e., the influence of boron or fluorine) are absent in nitrided oxide [15,94] suggesting that perhaps different mechanisms are involved. Similar to the case of pure oxide, approximately equal numbers of interface states and 'fixed' charge are seen in nitrided oxides [95].

Several theoretical attempts have been made to explain the microscopic role of nitrogen in NBTI, e.g., by calculating the energies for hole trapping at various defect structures. Analogous to the first reaction in Table 1, the reaction in the first row of Table 2 considers the reaction of holes and hydrogen with the silicon oxynitride structure. Calculations indicate that the reaction barrier decreases with the interfacial nitrogen concentration $x$ [22]. Considered differently as proton trapping on bonded nitrogen (second reaction in Table 1), the trap depth increases with $x$ [96]. Another reaction involving water and a nitrogen vacancy (Table 2, second row) has a lower reaction barrier [97]. A problem with all of these results, in our opinion, is that the focus on the reaction step ignores the fact that NBTI is diffusion limited. The results may be relevant to enhanced hole trapping in nitrided oxides, however, the calculated reaction barriers are very high, ~6–9 eV, so that none of the reactions would seem likely based on these results.

The focus of most work both theoretical (e.g., the reactions in Table 2) and experimental concerns nitrogen at the $Si/SiO_2$ interface, since it is widely accepted that this is the main contributor to NBTI [98]. Various processes are used to try to control the nitrogen profile in the oxide, to reduce the amount of N at the interface and incorporate more at the top, near the gate [41,72,94,99]. Fig. 12 shows the threshold voltage shift dependence on nitrogen concentration, measured by secondary ion mass spectroscopy in a 1.8 nm oxide [22,93,96]. For thicker oxides (5.2 nm) NBTI depends not only interfacial nitrogen, but also on the amount of nitrogen incorporated throughout the bulk [58]. Along this line, it has been proposed that nitrogen in the gate oxide may change the NBTI kinetics by inhibiting the transport of hydrogen away from the $Si/SiO_2$ interface [100].

EPR studies have shown that the density of $P_b$ centers is greatly reduced in nitrided oxides, and that these Si dangling bond centers can be completely eliminated with high enough nitrogen treatment (Fig. 13) [101]. This result goes opposite to the trend of increasing NBTI in nitrided oxides, strongly contradicting the assumption that $P_b$ centers are the origin of $N_{it}$. However, as shown in Fig. 14, negative bias stress on a ~1.7 nm oxynitride film caused depassivation of the $P_b$ centers, whose density in this case appeared nearly equal to the NBTI-induced interface states [57]. At intermediate nitrogen dose, the ratio of $P_{b1}$ to $P_{b0}$ centers varies and the spectrum changes slightly, suggesting that nitrogen causes structural changes at the interface [101,102].

Table 2
Nitrogen-related reactions

| Interface defect | Reaction | Refs. |
|---|---|---|
| $Si–H + Si_2–N–Si–(N_xO_{3-x})$ | $Si–H + Si_2–N–Si + h^+ \leftrightarrow Si^\cdot + Si^+ + Si–NH–Si$<br>alternatively, $H^+ + Si_2–N–Si \leftrightarrow Si_2–NH^+–Si$ | [22,96] |
| $H_2O + Si–Si–N_3$ | $Si–Si–N_3 + H_2O + h^+ \leftrightarrow Si–O–Si–NH^+–N_2 + H$<br>(free H then reacts with Si–H to leave dangling bond and molecular $H_2$) | [97] |

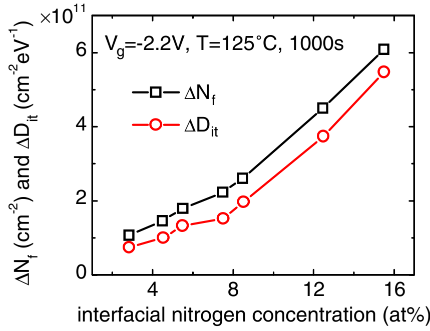


Fig. 12. Positive fixed charge ($\Delta N_f$) and interface state generation ($\Delta D_{it}$) after 1000 s of NBTI stress at the gate voltage of −2.2 V at 125 °C, as a function of interfacial nitrogen concentration measured by secondary ion mass spectroscopy. After [96].

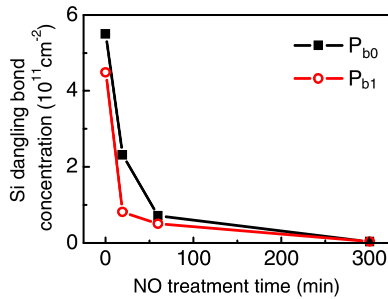


Fig. 13. Defect density measured in as-grown oxide (i.e., no electrical stress) in the unpassivated state, i.e., absence of H. After [101].

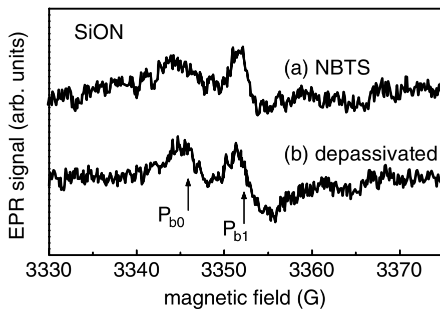


Fig. 14. Electron paramagnetic resonance signals (first derivative) of the $P_b$ centers in plasma-nitrided SiON/Si (a) after NBTI stress (b) thermally depassivated. The magnetic field is parallel to the [100] axis. Arrows indicate the positions of $P_{b0}$ and $P_{b1}$ centers. After [57].

Electrical measurements have shown that the energy distribution across the Si band gap of NBTI-induced interface states also varies with nitridation [103,104]. Nitrided oxides exhibit a higher interface state density near the Si conduction band edge, whereas pure $SiO_2$ exhibits more states at mid-gap and close to the Si valence band edge.

## 4. Applications

### 4.1. Circuit performance degradation

The negative threshold voltage ($V_t$) shift caused by NBTI results in lowered drive current for p-FETs, since the maximum drain current, for gate voltage equal to source–drain voltage ($V_g = V_{ds}$) is given approximately by [19,105]

$$I^{sat} = \mu_{eff} C_{ox} \frac{W}{L} (V_g - V_t)^{\theta} \quad (25)$$

for a transistor of width $W$, length $L$, and capacitance $C_{ox}$ per unit area. (We consider only long-channel devices in this discussion.) Typically $\theta$ ranges from 2 for long-channel devices to close to unity for short channels (<1 μm). Differentiating Eq. (25),

$$\frac{\Delta I^{sat}}{I^{sat}} = \theta \frac{-\Delta V_t}{(V_g - V_t)} \quad (26)$$

The frequency of a ring oscillator (a commonly used measure of technology performance, comprising a closed loop of an odd number of inverters) is

$$F \propto 1/\tau, \quad \tau \propto C V_{dd} \left[ \frac{1}{I_p^{sat}} + \frac{1}{I_n^{sat}} \right] \quad (27)$$

where $C$ is total input (gate) capacitance of each inverter. The two terms in the expression for $\tau$ describe the rise and fall times. Differentiating,

$$\frac{\Delta F}{F} = \frac{\Delta I_p^{sat}}{2 I_p^{sat}} - \frac{\Delta C}{C} \quad (28)$$

Ignoring the second term in Eq. (28) for the moment, Eqs. (26) and (28) show that the frequency degradation will be between 50% and 100% of the normalized $V_t$ shift. Eq. (26) assumes no change in the mobility, which is not strictly correct. The low-field mobility in particular is degraded because of Coulomb scattering from interface traps [19]. Thus, while these equations provide useful heuristics, more detailed numerical circuit models may be required for precise evaluation of the impact of NBTI.

According to Eq. (26) the circuit impact will be greater for lower operating voltage, because of the reduced 'head room' $V_g$–$V_t$ [34]. This can be measured as a change in the minimum circuit operation voltage ($V_{min}$) on product chips [106,107]. Other measures of performance degradation (e.g., $F_{max}$ decrease) on product chips have been shown to agree well with the trends associated with NBTI, such as the dependences on time

and temperature, weak dependence on channel length (corresponding to product speed sorting), and performance recovery after termination of the stress [108,109].

The generated interface traps also cause a small but measurable increase in the capacitance [19,34] and the subthreshold swing [41,110]. The capacitance contributes to the frequency degradation (Eq. (28)), and causes increased coupling of input to output, which has been shown to be important for analog applications [19,111]. For the most part, the increased $V_t$ results in lower off-state current, more than compensating the increased subthreshold swing. However in some cases the generated interface states can provide sufficient generation-recombination current to increase the off current and power consumption [18,112].

### 4.2. New materials and structures: High-κ and metal gate p-FETS

In recent years, there has been a great effort to integrate high dielectric constant (high-κ) materials and metal gates into FETs, in order to continue the scaling of FETs for future technologies. The potential reliability concerns for these new materials include NBTI as a major issue. The introduction of new materials into MOS technology also provides an opportunity to examine the materials dependence of reliability models and to test the predictions of theory.

$HfO_2$ is one of the leading high-κ candidates for the $SiO_2$ replacement and several different metals such as W, Re, TiN, TaN and are being explored for replacing poly silicon gates. Since NBTI is an important transistor reliability issue, NBTI in high-κ/metal-gate p-FETs is being investigated. It must be pointed out that the gate dielectric consists of a stack with an interfacial oxide plus $HfO_2$ layer. Experimental studies performed at elevated temperatures on $HfO_2$/metal p-FETS show that negative bias stressing causes $V_t$ to increase with a power-law dependence on stressing time which starts to saturate at longer time [113–115]. $\Delta V_t$, is also observed to increase with stressing bias and temperature. Measurements show that NBTI induced $\Delta V_t$ is accompanied by an increase in interfacial trap density ($\Delta N_{it}$), increase in subthreshold swing (ΔS) and decrease in peak transconductance ($\Delta g_m$) [113]. These observations for $\Delta V_t$, $\Delta N_{it}$, $\Delta S$ and $\Delta g_m$ are similar to those observed for conventional p-FETs with oxide and poly silicon gates.

Fig. 15 shows a comparison between NBTI data for p-FETs composed of oxynitride/$HfO_2$/W, oxynitride/$HfO_2$/TaN, and $SiO_2$/poly-Si. Since NBTI data are measured at various stress voltages and dielectric thickness, the comparison is made by plotting the increase in positive charge density ($\Delta Q = \Delta V_t \times C_{ox}$) at fixed stress time

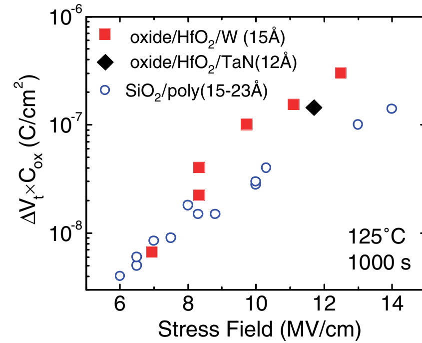


Fig. 15. Comparison between NBTI induced charge for p-FETs with $SiO_2$/poly gate [41], oxynitride/$HfO_2$/W [113], and oxynitride/$HfO_2$/TaN [115]. Equivalent oxide thickness (EOT) of various gate dielectric stacks are indicated in the legend.

and temperature vs. stress field. $\Delta Q$ calculated in this way assumes that the charge centroid is at the interface. The stress field is approximated as $V_g/t_{inv}$ where $t_{inv}$ is the equivalent oxide thickness calculated from the capacitance of the FET in inversion, $C_{inv} = 3.9\varepsilon_0/t_{inv}$. This relation roughly takes into account the fact that while the physical thickness for the high-κ dielectric is greater than that of $SiO_2$ for the same $t_{inv}$, most of the electric field falls across the interfacial oxide layer. As shown in Fig. 15, $HfO_2$ and $SiO_2$ stacks show similar $\Delta Q$ at various stress fields within the experimental scatter. It may be concluded that NBTI in high-κ/metal-gate p-FETs is similar to that in conventional oxide/poly p-FETs at elevated temperature.

There are some reports on negative bias stressing effect at room temperature that indicate that $\Delta V_t$ is dominated by hole trapping at existing traps in high-κ/metal p-FETs. In other words, no new traps are created during negative bias stressing and consequently interfacial trap density does not change with stressing at room temperature [116].

It is also interesting to investigate the NBTI effect in $SiO_2$/metal gate p-FETs. Only limited data are available for this system. A comparison of SiON/poly and SiON/W with $t_{ox} \sim 1.6$ nm found NBTI-induced $\Delta V_t$ to be the same for both poly silicon and W gates, for various stress fields at 125 °C [48].

In addition to studies for p-FETs with high-κ and metal gates, there are limited studies investigating the impact of silicon substrate orientation [104,117–119]. These studies have shown that NBTI is higher for ⟨110⟩ orientation in comparison to ⟨100⟩ orientation. This increase in NBTI attributed to higher density Si–H bonds at the Si/$SiO_2$ interface for ⟨110⟩ Si orientation. Aside from this, the majority of NBTI data for these new materials are similar to those for conventional p-FETs.

## 5. Conclusions

NBTI is a combination of positive trapped charge and interface state generation, resulting whenever negative gate bias is applied to a MOS structure. In spite of having been first reported nearly half a century ago, and notwithstanding a recent uptick in interest, many fundamental and practical questions remain.

Certain disagreements among published results, e.g., as to whether $V_t$ recovery involves $N_{it}$ or $N_f$ or both, may well be a result of differences among the samples used in various studies. Many such discrepancies may be caused by different nitrogen content, different oxide thickness, and/or other differences in processing of the dielectric or the gate material. We have not been able to completely root out these differences in this review. Since there are limited NBTI data for different metal gates in the literature, it cannot be concluded whether NBTI depends on the gate material.

The detailed understanding of the relaxation mechanism, whereby the $V_t$ shift recovers when the stress removed, is lacking. This is an area ripe for investigation. Deuterium isotope experiments could be useful here, in order to distinguish hydrogen motion from hole detrapping. Additional detailed studies of the temperature and field dependence of recovery are needed.

It is well established that the NBTI phenomenon is not dependent on current flow through the oxide, in contrast to oxide breakdown. However, as oxides have become thinner the increasing tunneling current can lead to additional defect generation which may have characteristics similar to NBTI, and which confuse the interpretation. The effect of tunneling current in thin oxides in causing $V_t$ instability in thin oxides needs further careful attention.

In the future, it may become more important to learn to distinguish defect generation from hole trapping at existing defects. For example, the relative contribution of hole trapping may be larger at room temperature compared to the usual accelerated stress conditions [104]. This is also critically important for understanding AC stress, and for developing a fundamental understanding of NBTI. The generation of interface states is an essential part of NBTI—charge trapping alone, without interface state generation, is considered a separate and distinct phenomenon—but the trapped charge component of NBTI is present and must be accounted for. Some of the models currently proposed either do not treat the trapped charge at all, or else assume a fixed relation between trapped charge and interface states. This is surely inadequate, so additional experimental work should drive an improved theoretical and practical understanding.

## Acknowledgements

We are grateful for helpful discussions with many people, especially (in alphabetical order): Ron Bolam, Anthony Chou, Toshiharu Furukawa, Terrence Hook, Meir Janai, Tassos Katsetos, Terrance Kueper, Giuseppe Larosa, Joe Lukaitis, Greg Massey, Steve Mittl, and Stewart Rauch. We also wish to thank Tak Ning, and Jeff Welser for motivating our interest in this subject.

## References

[1] Brozek T. Editorial, special issue on NBTI. Microelectron Reliab 2005;45:1–2.
[2] Peters L. NBTI: a growing threat to device reliability. In: Semiconductor International, 2004. p. 47–54.
[3] Nicollian EH, Brews JR. MOS (Metal Oxide Semiconductor) physics and technology. New York: John Wiley and Sons; 1982.
[4] Schroder DK, Babcock JA. Negative bias temperature instability: road to cross in deep submicron semiconductor manufacturing. Appl Phys Lett 2003;94:1–18.
[5] Miura Y, Matukura Y. Investigation of silicon–silicon dioxide interface using MOS structure. Jpn J Appl Phys 1966;5:180.
[6] Goetzberger A, Nigh HE. Surface charge after annealing of Al–$SiO_2$–Si structures under bias. Proc IEEE 1966;54: 1454.
[7] Goetzberger A, Lopez AD, Strain RJ. On the formation of surface states during stress aging of thermal Si–$SiO_2$ interfaces. J Electrochem Soc 1973;120:90–6.
[8] Deal BE, Sklar M, Grove AS, Snow EH. Characteristics of the surface-state charge ($Q_{ss}$) of thermally oxidized silicon. J Electrochem Soc 1967;114:266–74.
[9] Hofstein SF. Stabilization of MOS devices. Solid-State Electron 1967;10:657–70.
[10] Haller G, Knoll M, Braunig D, Wulf F, Fahrner WR. Bias-temperature stress on metal–oxide–semiconductor structures as compared to ionizing irradiation and tunnel injection. J Appl Phys 1984;56:1844–50.
[11] Breed DJ. A new model for the negative voltage instability in MOS devices. Appl Phys Lett 1975;26:116–8.
[12] Jeppson KO, Svensson CM. Negative bias stress of MOS devices at high electric fields and degradation of MNOS devices. J Appl Phys 1977;48:2004–14.
[13] Sinha AK, Smith TE. Kinetics of the slow-trapping instability at the Si/$SiO_2$ interface. J Electrochem Soc 1978;125:743–6.
[14] Ogawa S, Shimaya M, Shiono N. Impact of negative-bias temperature instability on the lifetime of single-gate CMOS structures with ultrathin (4–6 nm) gate oxides. Jpn J Appl Phys 1996;35:1484–90.
[15] Mitani Y, Nagamine M, Satake H, Toriumi A. Enhancement of $V_{th}$ degradation under NBT stress due to hole capturing. In: Extended abstracts of the 2003 international conference on solid state devices and materials; 2003. p. 16–7.

[16] Huard V, Monsieur F, Ribes G, Bruyere S. Evidence for hydrogen-related defects during NBTI stress in p-MOSFETs. In: 2003 International reliability physics symposium proceedings; 2003. p. 178–82.

[17] Rauch SE. The statistics of NBTI-induced $V_T$ and $\beta$ mismatch shifts in pMOSFETs. IEEE Trans Dev Mater Reliab 2002;2:89–93.

[18] Yamamoto T, Uwasawa K, Mogami T. Bias temperature instability in scaled p+ polysilicon gate p-MOSFETs. IEEE Trans Electron Dev 1999;46:921–6.

[19] Krishnan AT, Reddy V, Chakravarthi S, Rodriguez J, John S, Krishnan S. NBTI impact on transistor and circuit: models, mechanisms, and scaling effects. In: Digest of the 2003 international electron devices meeting; 2003. p. 349–52.

[20] Kimizuka N, Yamagachi K, Imai K, lizuka T, Liu CT, Keller RC, et al. NBTI enhancement by nitrogen incorporation into ultrathin gate oxide for 0.10 μm gate CMOS generation. In: Digest of the 2000 symposium on VLSI technology; 2000. p. 92–3.

[21] Ershov M, Lindley R, Saxena S, Shibkov A, Minehane S, Babcock J, et al. Transient effects and characterization methodology of negative bias temperature instability in p-MOS transistors. In: 2003 International reliability physics symposium proceedings; 2003. p. 606–7.

[22] Tan SS, Chen TP, Soon JM, Loh KP, Ang CH, Teo WY, et al. Neighboring effect in nitrogen-enhanced negative bias temperature instability. In: Extended abstracts of the 2003 international conference on solid state devices and materials; 2003. p. 70–1.

[23] Chen G, Li MF, Ang CH, Zheng JZ, Kwong DL. Dynamic NBTI of p-MOS transistors and its impact on MOSFET scaling. IEEE Electron Dev Lett 2002;23: 734–6.

[24] Chen G, Chuah KY, Li MF, Chan DSH, Ang CH, Zheng JZ, et al. Dynamic NBTI of PMOS transistors and its impact on device lifetime. In: 2003 International reliability physics symposium proceedings; 2003. p. 197–202.

[25] Tan SS, Chen TP, Ang CH, Teo WY, Chan L. New insights into dynamic negative bias temperature instability of p-MOSFETs. In: Extended abstracts of the 2003 international conference on solid state devices and materials; 2003. p. 68–9.

[26] Zhu B, Suehle JS, Bernstein JB. Mechanism for reduced NBTI effect under pulsed bias stress conditions. In: 2004 International reliability physics symposium proceedings; 2004. p. 689–90.

[27] Abadeer W, Ellis W. Behavior of NBTI under AC dynamic circuit conditions. In: 2003 International reliability physics symposium proceedings; 2003. p. 17–22.

[28] Ershov M, Saxena S, Karbasi H, Winters S, Minehane S, Babcock J, et al. Dynamic recovery of negative bias temperature instability in p-type metal–oxide–semiconductor field-effect transistors. Appl Phys Lett 2003;83: 1647–9.

[29] Kaczer B, Arkhipov V, Degraeve R, Collaert N, Groeseneken G, Goodwin M. Disorder-controlled-kinetics model for negative bias temperature instability and its experimental verification. In: 2005 International reliability physics symposium proceedings; 2005. p. 381–7.

[30] Huard V, Denais M. Hole trapping effect on methodology for DC and AC negative bias temperature instability measurements in p-MOS transistors. In: 2004 International reliability physics symposium proceedings; 2004. p. 40–5.

[31] Rangan S, Mielke N, Yeh ECC. Universal recovery behavior of negative bias temperature instability. Digest of the 2003 international electron devices meeting; 2003. p. 341–4.

[32] Denais M, Huard V, Parthasarathy C, Ribes G, Perrier F, Revil N, et al. New methodologies of NBTI characterization eliminating recovery effects. In: Proceedings of ESSDERC; 2004. p. 265–8.

[33] Denais M, Bravaix A, Huard V, Parthasarathy C, Ribes G, Perrier F, et al. On-the-fly characterization of NBTI in ultra-thin gate oxide PMOSFETs. In: Digest of the 2004 international electron devices meeting; 2004. p. 109–12.

[34] Reddy V, Krishnan AT, Marshall A, Rodriguez J, Natarajan S, Rost T, et al. Impact of negative bias temperature instability on digital circuit reliability. In: 2002 International reliability physics symposium proceedings; 2002. p. 248–54.

[35] Ang DS, Pey KL. Evidence for two distinct positive trapped charge components in NBTI stressed p-MOSFETs employing ultrathin CVD nitride gate dielectric. IEEE Electron Dev Lett 2004;25:637–9.

[36] DiMaria DJ, Stasiak JW. Trap creation in silicon dioxide produced by hot electrons. J Appl Phys 1989;65:2342–56.

[37] Huard V, Denais M, Perrier F, Parthasarathy CR. Static and dynamic NBTI stress in pMOS transistors. In: INFOS. Barcelona; 2003.

[38] Denais M, Huard V, Parthasarathy C, Ribes G, Perrier F, Revil N, et al. Interface trap generation and hole trapping under NBTI and PBTI in advanced CMOS technology with a 2 nm gate oxide. IEEE Trans Dev Mater Reliab 2004;4:715–22.

[39] Huard V, Denais M, Perrier F, Revil N, Parthasarathy C, Bravaix A, et al. A thorough investigation of MOSFETs NBTI degradation. Microelectron Reliab 2005;45:83–98.

[40] Lin HC, Lee DY, Ou SC, Chien CH, Huang TY. Impacts of hole trapping on the NBTI degradation and recovery in PMOS devices. In: Extended abstracts of the international workshop on gate insulators (IWGI2003); 2003. p. 76–9.

[41] Tsujikawa S, Mine T, Watanabe K, Shimamoto Y, Tsuchiya R, Ohnishi K, et al. Negative bias temperature instability of p-MOSFETs with ultra-thin SiON gate dielectics. In: 2003 International reliability physics symposium proceedings; 2003. p. 183–8.

[42] Tsujikawa S, Watanabe K, Tsuchiya R, Ohnishi K, Yugami J. Experimental evidence for the generation of bulk traps by negative bias temperature stress and their impact on the integrity of direct-tunneling gate dielectrics. In: Digest of the 2003 symposium on VLSI technology; 2003. p. 139–40.

[43] Mahapatra S, Alam MA, Kumar PB, Dalei TR, Saha D. Mechanism of negative bias temperature instability in CMOS devices: degradation, recovery and impact of nitrogen. In: Digest of the 2004 international electron devices meeting; 2004. p. 105–8.

[44] Akbar MS, Agostinelli M, Rangan S, Lau S, Castillo C, Pae S, et al. PMOS thin gate oxide recovery upon negative

bias temperature stress. In: 2004 International reliability physics symposium proceedings; 2004. p. 683–4.
[45] Aono H, Murakami E, Okuyama K, Nishida A, Minami M, Ooji Y, et al. Modeling of NBTI degradation and its impact on electric field dependence of the lifetime. In: 2004 International reliability physics symposium proceedings; 2004. p. 23–7.
[46] Liu CH, Lee MT, Lin CY, Chen J, Schruefer K, Brighten J, et al. Mechanism and process dependence of negative bias temperature instability (NBTI) for p-MOSFETs with ultrathin gate dielectrics. In: Digest of the 2001 international electron devices meeting; 2001. p. 861–4.
[47] Stojadinović N, Danković D, Djorić-Veljković S, Davidović V, Manić I, Golubović S. Negative bias temperature instabilities in p-channel Power VDMOSFETs. Microelectron Reliab 2005;45:1343–8.
[48] Zafar S. Statistical mechanics based model for negative bias temperature instability induced degradation. J Appl Phys 2005;97:103709-9.
[49] Zafar S, Lee BH, Stathis JH, Ning TH. A model for negative bias temperature instability (NBTI) in oxide and high *k* p-FETs. In: Digest of the 2004 symposium on VLSI technology; 2004. p. 208–9.
[50] Blat CE, Nicollian EH, Poindexter EH. Mechanism of negative-bias temperature instability. J Appl Phys 1991;69:1712–20.
[51] Noyori M, Ishihara T, Higuchi H. Secondary slow trapping—a new moisture induced instability phenomenon in scaled CMOS devices. In: 1982 International reliability physics symposium proceedings; 1982. p. 113–21.
[52] Sasada K, Arimoto M, Nagasawa H, Nishida A, Aoe H, Dan T, et al. The influence of SiN films on negative bias temperature instability and characteristics in MOSFETs. In: Proceedings of international test conference; 1998. p. 207–10.
[53] Lee DY, Lin HC, Chiang WJ, Lu WT, Huang GW, Huang TY, et al. Process and doping species dependence of negative-bias-temperature instability for p-channel MOSFETs. In: 2002 Symposium on plasma- and process-induced damage; 2002. p. 150–3.
[54] Lee J-S, Lyding JW, Hess K. Hydrogen-related extrinsic oxide trap generation in thin gate oxide film during negative-bias temperature instability stress. In: 2004 International reliability physics symposium proceedings; 2004. p. 685–6.
[55] Hess DW. Effect of chlorine on the negative bias instability in MOS structures. J Electrochem Soc 1977; 124:740–3.
[56] Hook TB, Adler E, Guarin F, Lukaitis J, Rovedo N, Schruefer K. The effects of fluorine on parametrics and reliability in a 0.18 μm 3.5/6.8 nm dual gate oxide CMOS technology. IEEE Trans Electron Dev 2001;48:1346–53.
[57] Fujieda S, Miura Y, Saitoh M, Hasegawa E, Koyama S, Ando K. Interface defects responsible for negative-bias temperature instability in plasma-nitrided SiON/Si(1 0 0) systems. Appl Phys Lett 2003;82:3677–9.
[58] Hook TB, Bolam R, Clark W, Burnham J, Rovedo N, Schutz L. Negative bias temperature instability on three oxide thicknesses (1.4/2.2/5.2 nm) with nitridation variations and deuteration. Microelectron Reliab 2005;45: 47–56.
[59] Makabe M, Kubota T, Kitano T. Bias-temperature degradation of p-MOSFETs: mechanism and suppression. In: 2000 International reliability physics symposium proceedings; 2000. p. 205–9.
[60] Ogawa S, Shiono N. Generalized diffusion-reaction model for the low-field charge-buildup instability at the Si–$SiO_2$ interface. Phys Rev B 1995;51:4218–30.
[61] Alam MA, Mahapatra S. A comprehensive model of PMOS NBTI degradation. Microelectron Reliab 2005;45: 71–81.
[62] Kaczer B, Arkhipov V, Degraeve R, Collaert N, Groeseneken G, Goodwin M. Temperature dependence of the negative bias temperature instability in the framework of dispersive transport. Appl Phys Lett 2005;86:143506.
[63] Chakravarthi S, Krishnan AT, Reddy V, Machala CF, Krishnan S. A comprehensive framework for predictive modeling of negative bias temperature instability. In: 2004 International reliability physics symposium proceedings; 2004. p. 273–82.
[64] Ogawa S, Shimaya M, Shiono N. Interface-trap generation at ultra-thin $SiO_2$ (4–6 nm)-Si interfaces during negative-bias temperature aging. J Appl Phys 1995;77: 1137–48.
[65] Mahapatra S, Kumar PB, Alam MA. A new observation of enhanced bias temperature instability in thin gate oxide p-MOSFETs. In: Digest of the 2003 international electron devices meeting; 2003. p. 337–41.
[66] Houssa M, Autran JL, Stesmans A, Heyns MM. Model for interface defect and positive charge generation in ultrathin $SiO_2/ZrO_2$ gate dielectric stacks. Appl Phys Lett 2002;81:709–11.
[67] Houssa M, Aoulaiche M, De Gendt S, Groeseneken G, Heyns MM. Reaction-dispersive proton transport model for negative bias temperature instabilities. Appl Phys Lett 2005;86:093506.
[68] Krishnan MS, Kol'dyaev V. Modeling kinetics of gate oxide reliability using stretched exponents. In: 2002 International reliability physics symposium proceedings; 2002. p. 421–2.
[69] Jackson WB. Connection between the Meyer–Neldel relation and multiple-trapping transport. Phys Rev B 1988;38:3595–8.
[70] Yelon A, Movaghar B. Microscopic explanation of the compensation (Meyer–Neldel) rule. Phys Rev Lett 1990; 65:618–20.
[71] Haggag A, McMahon W, Hess K, Cheng K, Lee J, Lyding J. High-performance chip reliability from short-time-tests. In: 2001 International reliability physics symposium proceedings; 2001. p. 271–9.
[72] Mitani Y. Influence of nitrogen in ultra-thin SiON on negative bias temperature instability under AC stress. In: Digest of the 2004 international electron devices meeting; 2004. p. 117–20.
[73] Alam MA. A critical examination of the mechanics of dynamic NBTI for PMOSFETs. In: Digest of the 2003 international electron devices meeting; 2003. p. 345–8.
[74] Usui H, Kanno M, Morikawa T. Time and voltage dependence of degradation and recovery under pulsed

negative bias temperature stress. In: 2003 International reliability physics symposium proceedings; 2003. p. 610–1.
[75] Poindexter EH. MOS interface states: overview and physiochemical perspective. Semicond Sci Technol 1989; 4.
[76] Gerardi C, Poindexter EH, Caplan PJ, Harmatz M, Buchwald WR. Generation of $P_b$ centers by high electric fields: thermochemical effects. J Electrochem Soc 1989; 136:2609–14.
[77] Gerardi C, Poindexter EH, Harmatz M, Warren WL, Nicollian EH, Edwards AH. Depassivation of damp-oxide $P_b$ centers by thermal and electric field stress. J Electrochem Soc 1991;138:3765–70.
[78] Tsetseris L, Zhou XJ, Fleetwood DM, Schrimph RD, Pantelides ST. Physical mechanisms of negative-bias temperature instability. Appl Phys Lett 2005;86:142103.
[79] Mahapatra S, Alam MA. A predictive reliability model for PMOS bias temperature degradation. In: Digest of the 2002 international electron devices meeting; 2002. p. 505–8.
[80] Griscom DL. Hydrogen model for radiation-induced interface states in $SiO_2$-on-Si structures: a review of the evidence. J Electron Mater 1982;21:763–7.
[81] Szekeres A, Alexandra S. Low-temperature treatment of $Si/SiO_2$ structures in an RF hydrogen plasma. Vacuum 1996;47:1483–6.
[82] Sah C-T, Sun JY-C, Tzou JJ-T. Deactivation of the boron acceptor in silicon by hydrogen. Appl Phys Lett 1983;43:204–6.
[83] Mitani Y, Nagamine M, Satake H, Toriumi A. NBTI mechanism in ultra-thin gate dielectric: nitrogen-originated mechanism in SiON. In: Digest of the 2002 international electron devices meeting; 2002. p. 509–12.
[84] Chen MG, Li JS, Jiang C, Liu CH, Su KC, Chang YJ. NBTI mechanism explored on the back gate bias for pMOSFETs. In: 2003 Integrated reliability workshop final report; 2003. p. 131–2.
[85] Chen SJ, Lin CC, Chung S, Lin JC, Chu CH. Reliability test guidelines for a 0.18 μm generation multi-oxide CMOS technology for system-on-chip applications. Jpn J Appl Phys 2003;42:1928–32.
[86] Brower KL. Dissociation kinetics of hydrogen-passivated (1 1 1) Si–$SiO_2$ interface defects. Phys Rev B 1990;42: 3444–53.
[87] Cartier E, Stathis JH, Buchanan DA. Passivation and depassivation of silicon dangling bonds at the $Si/SiO_2$ interface by atomic hydrogen. Appl Phys Lett 1993;63: 1510–2.
[88] Stathis JH, Cartier E. Atomic hydrogen reactions with $P_b$ centers at the (1 0 0) $Si/SiO_2$ interface. Phys Rev Lett 1994;72:2745–8.
[89] Stathis JH, Cartier E, Edwards AH, Poindexter EH. The $P_{b1}$ center at the Si–$SiO_2$ interface: updated evidence and emerging models. In: Deen MJ et al., editors. Silicon nitride and silicon dioxide thin insulating films. Pennington, NJ: The Electrochemical Society; 1997. p. 259–74.
[90] Cartier E, Stathis JH. Hot-electron induced passivation of silicon dangling bonds at the Si (1 1 1)/$SiO_2$ interface. Appl Phys Lett 1996;69:103–5.
[91] DiMaria DJ, Stathis JH. Trapping and trap creation studies on nitrided and reoxidized-nitrided silicon dioxide films on silicon. J Appl Phys 1991;70:1500–9.
[92] Shiau W-T, Terry FL. Bias-temperature stability of nitrided oxides and reoxidized nitrided oxides. J Electron Mater 1989;18:767–73.
[93] Tan SS, Chen TP, Ang CH, Chan L. Relationship between interfacial nitrogen concentration and activation energies of fixed-charge trapping and interface state generation under bias-temperature stress condition. Appl Phys Lett 2003;82:269–71.
[94] Ang CH, Lek CM, Tan SS, Cho BJ, Chen T, Lin W, et al. Negative bias temperature instability on plasma-nitrided silicon dioxide film. Jpn J Appl Phys 2002;41:L314–6.
[95] Tan SS, Chen TP, Ang CH, Chan L. Mechanism of nitrogn-enhanced negative bias temperature instability in pMOSFET. Microelectron Reliab 2005;45:19–30.
[96] Tan SS, Chen TP, Soon JM, Loh KP, Ang CH, Teo WY, et al. Linear relationship between $H^+$-trapping reaction energy and defect generation: Insight into nitrogen-enhanced negative bias temperature instability. Appl Phys Lett 2003;83:530–2.
[97] Ushio J, Maruizumi T. Interface structures generated by negative-bias temperature instability in $Si/SiO_2$ and $SiO_xN_y$ interfaces. Appl Phys Lett 2002;81:1818–20.
[98] Tan SS, Chen TP, Ang CH, Tan YL, Chan L. Influence of nitrogen proximity from the $Si/SiO_2$ interface on negative bias temperature instability. Jpn J Appl Phys 2002;41: L1031-L3.
[99] Sasaki T, Kuwazawa K, Tanaka K, Kato J, Kwong DL. Engineering of nitrogen profile in an ultrathin gate insulator to improve transistor performance and NBTI. IEEE Electron Dev Lett 2003;24:150–2.
[100] Kaczer B, Arkhipov V, Jurczak M, Groeseneken G. Negative bias temperature instability (NBTI) in $SiO_2$ and SiON gate dielectrics understood through disorder-controlled kinetics. Microelectron Eng 2005;80:122–5.
[101] Gosset LG, Ganem JJ, von Bardeleben HJ, Rigo S, Trimaille I, Cantin JL, et al. Formation of modified Si/ $SiO_2$ interfaces with intrinsic low defect concentrations. J Appl Phys 1999;85:3661–5.
[102] Miura Y, Fujieda S. Nitridation effects on $P_b$ center structures at $SiO_2$/Si (1 0 0) interfaces. J Appl Phys 2004;95:4096–101.
[103] Stathis JH, LaRosa G, Chou A. Broad energy distribution of NBTI-induced interface states in p-MOSFETs with ultra-thin nitrided oxide. In: 2004 International reliability physics symposium proceedings; 2004. p. 1–7.
[104] Stathis JH, Bolam R, Yang M, Hook TB, Chou A, Larosa G. Interface state generation in p-FETs with ultra-thin oxide and oxynitride on (1 0 0) and (1 1 0) Si substrates. Microelectron Eng 2005;80:126–9.
[105] Taur Y, Ning TH. Fundamentals of modern VLSI devices. Cambridge: Cambridge University Press; 1998.
[106] Lee Y-H, Mielke N, Sabi B, Stadler S, Nachman R, Hu S. Effect of pMOST bias-temperature instability on circuit reliability performance. In: Digest of the 2003 international electron devices meeting; 2003. p. 353–6.
[107] Mueller K, Gupta S, Pae S, Agostinelli M, Aminzadeh P. 6-T cell circuit dependent GOX SBD model for accurate

prediction of observed Vccmin test voltage dependency. In: 2004 International reliability physics symposium proceedings; 2004. p. 426–9.

[108] Bolam R. Tutorial on product reliability challenges for semiconductor VLSI technology. In: 2004 International reliability physics symposium proceedings. Phoenix, AZ; 2004.

[109] Reddy V, Carulli J, Krishnan AT, Bosch W, Burgess B. Impact of negative bias temperature instability on product parameter drift. In: Proceedings of international test conference; 2004. p. 148–55.

[110] Krishnan AT, Krishnan S, Reddy V. Impact of charging damage on negative bias temperature instability. In: Digest of the 2001 international electron devices meeting; 2001. p. 865–8.

[111] Krishnan AT. Tutorial on NBTI: process, device, and circuit. In: 2005 International reliability physics symposium proceedings. San Jose, CA; 2005.

[112] Ghodsi R, Sharifzadeh S, Majjiga J. Gate-induced drain-leakage in buried-channel PMOS—a limiting factor in development of low-cost, high-performance 3.3 V, 0.25 μm technology. IEEE Electron Dev Lett 1998;19: 354–6.

[113] Zafar S, Lee BH, Stathis JH. Evaluation of NBTI in $HfO_2$ gate-dielectric stacks with tungsten gates. IEEE Electron Dev Lett 2004;25:153–5.

[114] Houssa M, Aoulaiche M, Van Elshocht S, De Gendt S, Groeseneken G, Heyns MM. Impact of Hf content on negative bias temperature instabilities in HfSiON-based gate stacks. Appl Phys Lett 2005;86:173509–12.

[115] Choi R, Onishi K, Kang CS, Gopalan S, Nieh R, Kim YH, et al. Fabrication of high quality ultra thin $HfO_2$ gate dielectric MOSFETs using deuterium anneals. In: Digest of the 2002 international electron devices meeting; 2002. p. 613–7.

[116] Lu W-T, Lin P-C, Huang T-Y, Chien C-H, Yang M-J, Huang I-J, et al. The characteristics of hole trapping in $HfO_2/SiO_2$ gate dielectrics with TiN gate electrode. Appl Phys Lett 2004;85:3525–7.

[117] Momose HS, Ohguro T, Kojima K, Nakamura S, Toyoshima Y. 1.5 nm gate oxide CMOS on [110] surface-oriented Si substrate. IEEE Trans Electron Dev 2003;50:1001–4.

[118] Maeda S, Choi J-A, Yang J-H, Jin Y-S, Bae S-K, Kim Y-W, et al. Negative bias instability in triple gate transistors. In: 2004 International reliability physics symposium proceedings; 2004.

[119] Zafar S, Yang M, Gusev E, Callegari A, Stathis J, Ning T, et al. A comparative study of NBTI as a function of Si substrate orientation and gate dielectrics (SiON and SiON/$HfO_2$). In: Proceedings of IEEE VLSI-TSA; 2005. p. 128–9.